Guerra, A., Guidi, F., Clemente, A., D'Errico, R., Dussopt, L., & Dardari, D. (2015). Application of transmitarray antennas for indoor mapping at millimeter-waves. In 2015 European Conference on Networks and Communications (EuCNC) (pagg. 77–81). https://doi.org/10.1109/EuCNC.2015.7194044

Application of Transmitarray Antennas for Indoor Mapping at Millimeter-Waves

Anna Guerra*, Francesco Guidi*, Antonio Clemente†‡, Raffaele D'Errico†‡,
Laurent Dussopt†‡, and Davide Dardari*

*DEI, University of Bologna, via Venezia 52, I-47521 Cesena (FC), Italy
{anna.guerra3, f.guidi, davide.dardari}@unibo.it
†Univ. Grenoble-Alpes, 38000 Grenoble, France, ‡CEA, LETI, MINATEC Campus, 38054 Grenoble, France
{antonio.clemente, raffaele.derrico, laurent.dussopt}@cea.fr

***Abstract*—Millimeter-waves are expected to play a key role in next 5G scenario due to the availability of a large clean unlicensed bandwidth at 60 GHz and the possibility to realize packed antenna arrays, with a consequent increase of the communication capacity and the introduction of new functionalities, such as high-definition localization and personal radar for automatic environment mapping. In this paper we propose the adoption of millimeter-wave transmitarrays for personal radar applications and we investigate the impact of the radiation pattern characteristics on the map reconstruction accuracy, by analysing how the number of array elements, of quantization bits and the focal distance affect the environment reconstruction performance.**

***Index Terms*—Transmitarray antennas, indoor mapping, millimeter-wave, personal radar.**

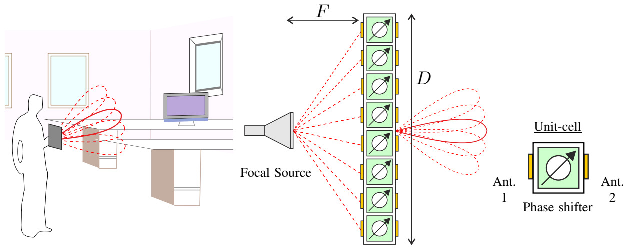

(a) (b) (c)

Fig. 1. Personal radar mapping application (a), TA structure (b), unit-cell (c).

I. INTRODUCTION

In the Internet of Things context, people, devices and objects are expected to be interconnected and to share information enabling environment-related applications and allowing a mapping of the real world into the internet space [1]. Moreover, fifth generation (5G) mobile networks will cope with the necessity to achieve an ubiquitous positioning, independent navigation and mapping capabilities not only outdoor but also in shadowed or GPS-denied environments as, for example, inside buildings.

Traditionally, simultaneous localization and mapping (SLAM) techniques permit to automatically reconstruct a 2D/3D map of an unknown environment and to self-localize using robots. Typically, the map reconstruction is achieved thanks to mechanical-steered laser, camera or microwave-based sensors [2]. Nevertheless, in accordance with the 5G vision, an emerging and more appealing solution to provide high ranging accuracy and fine angular resolution is represented by the combination of massive antenna array and millimeter-wave (mmW) technologies [3], [4]. In fact, thanks to the reduced wavelength, it will be possible to embed a small-size/portable radar with a massive antenna array able to electronically steer its beam and, subsequently, to scan the area to be mapped [5]. Following this principle, the idea of a *personal radar* has been recently proposed as a smartphone-centric low cost solution for the navigation and mapping problem in [5], [6] (Fig. 1-(a)).

Among the current different antenna arrays technologies, transmitarrays (TAs) could be a feasible solution to be incorporated in a personal radar system. A pictorial depiction of the TA is reported in Fig. 1-(b). TAs consist of a focal source illuminating a planar array whose building block are the unit-cells. As reported in Fig. 1-(c), each unit-cell consists of two antennas (indicated as Ant. 1 and 2) connected by a phase shifter. By tuning the transmission phase of the array elements, it is possible to obtain a specific phase distribution across the TA aperture and thus, to perform real-time beamsteering or beamforming by focusing, collimating, or shaping the incident power on the array in any direction in the free space. The TA is able to operate both in transmission and receive mode.

Thanks to their spatial feeding technique, TAs are extremely competitive compared to traditional phased arrays in terms of cost, complexity and power consumption. Unlike reflectarray antennas [7], TAs are free from focal source masking effects. Theoretical and experimental studies have been conducted to characterize and fully describe TAs [8]–[10]. Moreover, several electronically reconfigurable unit-cells and TAs have been proposed from the C- to the Ka-band using varactors diodes [11], phase shifters [12], PIN diodes [13], [14], or microelectromechanical system devices (MEMS) [15].

Motivated by this context, in this paper we investigate the application of the TA technology for indoor mapping by using a Bayesian approach. The theoretical array radiation characteristics are taken into account during the map estimation process. In particular, the mapping capabilities are analysed as a function of the number of antenna elements, the focal distance (F) and the quantization effect arising when only a

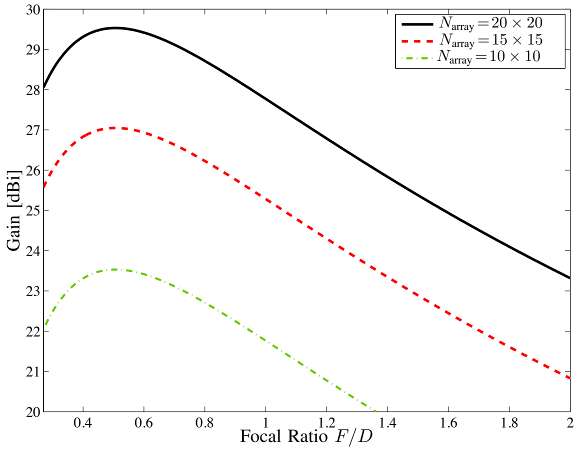

Fig. 2. Theoretical gain of $N_{\text{array}} = 10 \times 10$, 15×15 and 20×20 TA as a function of the focal ratio at $f_0 = 60$ GHz.

discrete set of phase shifts is available.

II. MILLIMETER-WAVE TRANSMITARRAY MODEL

In this section, the TA model used in our investigation is presented. The TA radiation properties (i.e. radiation pattern as a function of the steering angle and frequency) have been extracted using an *ad-hoc* simulator experimentally validated in previous works at X-, Ka-, and V-band [8]–[10], [13].

We here consider an ideal TA configuration at $f_0 = 60$ GHz with lossless and matched elements (i.e. the efficiency of the focal source η_{FS} and that of the unit-cells η_{IL} are both equal to 100%) in order to evaluate the best performance of such TAs for mapping purposes.

The focal source has been modelled with a generic $\cos^n(\theta)$ radiation pattern with n being the focal source order [16]. Note that the directivity varies as a function of n: the transition from $n = 1$ to $n = 10$ results in a directivity increase from $D_{\text{FS}} = 6$ dBi to $D_{\text{FS}} = 13.4$ dBi. In the following, we will assume a focal source order of $n = 4$ representative of a standard gain horn with a directivity of 10 dBi, that is a typical choice for TAs [8]–[10], [13].

The linearly polarized unit-cell is modelled as a uniform aperture as described in [16]. Ideally, a continuous phase shift between $0°$ and $360°$ is necessary to exactly compensate the phase on the array aperture at the cost of a higher complexity and losses in the case of electronically reconfigurable TA. A phase quantization can be introduced to avoid these drawbacks. Therefore, in our analysis, arrays with a 1-, 2-, 3-bit phase quantization have been considered.

Denoting with N_x (N_y) the number of unit-cells elements in the x- (y-) direction and considering an inter-element spacing of $d_x = d_y = \lambda_0/2$, where λ_0 is the wavelength at f_0 (i.e. $\lambda_0 = 5$ mm at the center frequency 60 GHz), the TA side is set to $D = N_x d_x = N_y d_y$ (e.g. if the number of array elements is $N_{\text{array}} = N_x \times N_y = 15 \times 15$, then the side will be 37.5 mm).

One of the most important parameter in the design of the TA is the F/D ratio. The F/D ratio could be optimized by maximizing the TA gain, or equivalently, by finding the best trade-off between spillover losses and tapper efficiency. Indeed, when F/D is higher than the optimum value (in terms of maximum gain) and the focal source is too distant from the receiving array, a great part of the power emitted by the focal source is not intercepted by the array aperture (spillover loss). On the contrary, when the focal source is close, the array surface is bad illuminated (low tapper efficiency). In Fig. 2, the simulated gains considering a perfect phase compensation and different sized TAs are reported as a function of the F/D ratio. The optimum $(F/D)_{\text{opt}}$ is between 0.4 and 0.5 and it corresponds to different optimum focal distance values $F_{\text{opt}} = 25$ mm, $F_{\text{opt}} = 19$ mm, $F_{\text{opt}} = 13$ mm for $N_{\text{array}} = 20 \times 20$, $N_{\text{array}} = 15 \times 15$ and $N_{\text{array}} = 10 \times 10$, respectively. It is important to underline that the F/D ratio plays a key role on the integrability of the TA in portable devices as it defines the total volume occupied by the array. As a consequence, the effect of a reduced focal distance will be analysed to evaluate how a gain degradation impacts the mapping performance.

TABLE I
THEORETICAL PERFORMANCE OF TRANSMITARRAYS OPTIMIZED AT $f_0 = 60$ GHZ FOR MAXIMUM GAIN AND DIFFERENT PHASE COMPENSATION CONDITIONS. THE STEERING DIRECTION IS $\theta_0 = 0°$.

	G [dBi]	SLL [dB]	HPBW [Degrees]	$(F/D)_{\text{opt}}$
Perfect	27.05	23.27	8	0.5
3 bits	26.88	24.62	8	0.44
2 bits	26.35	20.62	8	0.45
1 bit	23.53	20.25	9	0.49

In Table I, a comparison of the performance at $f_0 = 60$ GHz of the 15×15 TA is reported as a function of the number of bits used for the phase compensation process. The steering direction is here considered fixed to $\theta_0 = 0°$. The obtained performance considering the perfect phase compensation are also reported as a benchmark. It can be seen that the non-ideal phase compensation impacts the performance of the TA. Specifically, the maximum gain $G(\theta_0, f_0)$ decreases (quantization loss on directivity) while the level of the secondary lobes increases. The side lobe level (SLL) represents the difference (in [dB]) between the maximum gain and the peak of the main side lobe which has been reported in the Table I. The half power beamwidth (HPBW) is here computed at f_0, which is a quite good approximation, despite the considered bandwidth $W = 1$ GHz, because of the high f_0 involved. In the following, we consider only 2 bits for phase compensation (four different discrete phase values: $0°$, $90°$, $180°$, and $270°$) that is, in our opinion, a good compromise between structure complexity and radiation efficiency for an electronically reconfigurable TA.

Due to all the aforementioned characteristics, TA antennas represent excellent candidates for environmental mapping applications at mmW. In particular, for the following mapping analysis, we define $\theta_b = -\pi/2 \left(\frac{N_{\text{steer}}-1}{N_{\text{steer}}}\right) + (b-1)2\pi/3N_{\text{steer}}$, $b = 1, 2, \ldots N_{\text{steer}}$, being the set of N_{steer} steering directions considered during the scanning process. Note that the maximum steering angle is set to $60°$ according to the results

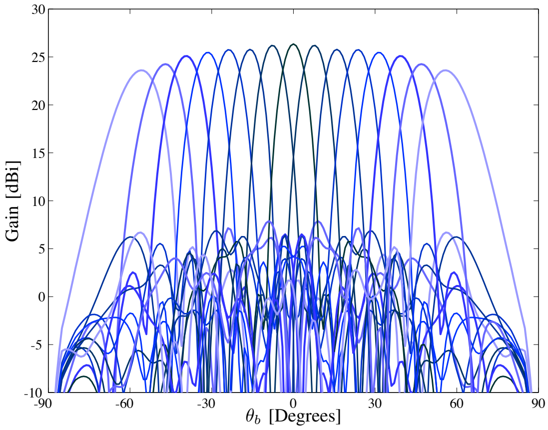

Fig. 3. Gain of 2-bit 15×15 TA as a function of the steering angle θ_b at $f_0 = 60\,\text{GHz}$ and for $(F/D)_{\text{opt}}$ ratio.

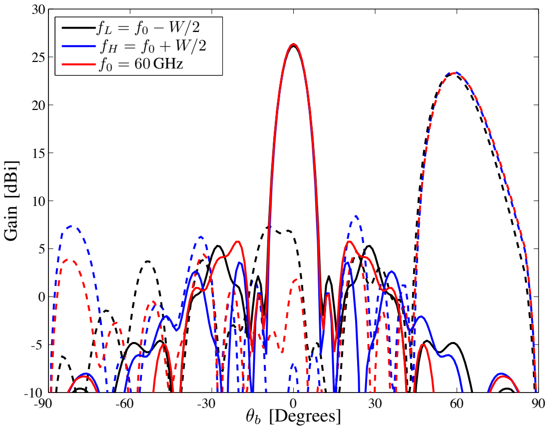

Fig. 4. Theoretical gain of 2-bit 15×15 TA as a function of the steering angle θ_b with $W = 1\,\text{GHz}$ and for $(F/D)_{\text{opt}}$ ratio. Continuous lines refers to the case $\theta_b = 0°$, dashed lines refers to the case $\theta_b = 60°$

reported in Fig. 3 for a 2-bit 15×15 TA. In Fig. 4 the theoretical gain of the 15×15 TA has been reported for two steering angles θ_b, namely $0°$ (continuous lines) and $60°$ (dashed lines) and for three frequencies in the considered band (lowest, central and highest frequencies). As previously mentioned, with a large bandwidth a slight difference in the radiation characteristic can be observed due to beamsquinting effect. However, as the fractional bandwidth W/f_0 is small, this effect is limited.

III. TRANSMITARRAY ANTENNAS FOR PERSONAL RADAR ENVIRONMENTAL MAPPING

In the following, we adopt a state-space model for probabilistic mapping [5] where the TA radiation characteristics previously described, are included. In particular, the TA is assumed to be embedded in a portable radar and to scan the environment thanks to its beamsteering capacity in order to collect the environmental response in form of backscattered energy measurements as proposed in [5].

In accordance with a grid-based scheme, the environment to be mapped is discretized in $N_{\text{L}} = X_{\text{grid}} Y_{\text{grid}}$ cells, where each cell is associated with a radar cross section (RCS) value to be inferred by the estimation process. The cell size is set in accordance to the minimum footprint area (e.g. a discretization of $0.2 \times 0.2\,\text{m}^2$ corresponds to the footprint area of a 20×20 TA at a distance of $d = 0.5\,\text{m}$). Moreover, differently from conventional approaches where a preliminary detection phase is provided, we adopt a 1-step approach where all the available raw energy measurements are included in the observation model. In the following, some highlights of the mapping algorithm are reported, but for further details refer to [5].

1) State Vector: Differently from SLAM approaches, we assume here that the radar position and orientation have not to be inferred by the estimation process as they are provided by external localization sensors. Therefore, the state of the system is only composed by the map parameters of interest and it is described by the state vector as

$$\mathbf{x}(k) = \mathbf{m}(k) = [m_1(k), \ldots, m_i(k), \ldots, m_{N_{\text{L}}}(k)]^{\text{T}} \quad (1)$$

where k is the discrete time instant and $m_i(k)$ indicates the root radar cross section (RRCS) (with sign) of the ith cell of the grid. Obviously, if the cell is empty (only air), the corresponding RRCS is zero. Moreover, we neglect the dependency of $m_i(k)$ from the frequency and we consider a stationary environment so that a transition model is not introduced.

2) Observation Model: As previously anticipated, the TA provides a rich set of energy observations starting from the signals backscattered by the surrounding environment for different steering directions. In fact, a non-coherent scheme is here adopted to reduce the complexity and to deal with the a-priori lack of knowledge on environment electromagnetic characteristics [5]. The interrogation signal for each steering direction is composed of N_{p} pulses and energy measurements are taken during the time frame T_{f} starting after the transmission of each pulse by subdividing the time frame into $N_{\text{bin}} = \lfloor T_{\text{f}}/T_{\text{ED}} \rfloor$ time slots (bins) of duration $T_{\text{ED}} \approx 1/W$.

Define $\mathbf{e}(k)$ the vector containing the accumulated measured energy at the output of the receiver at time k

$$\begin{aligned}\mathbf{e}(k) = &[e_{11}(k), \ldots, e_{1N_{\text{bin}}}(k), \ldots, e_{bs}(k), \ldots, \\ &e_{N_{\text{steer}}1}(k), \ldots\, e_{N_{\text{steer}}N_{\text{bin}}}(k)]^{\text{T}}\end{aligned} \quad (2)$$

where $e_{bs}(k)$ represents the accumulated energy measurement in the sth time bin and bth steering angle θ_b.

As shown in [5], $e_{bs}(k)$ can be approximated with a Gaussian distribution for large N_{p}. Thanks to this property, it is possible to derive a Gaussian observation model of the state-space model as

$$\begin{aligned}\mathbf{z}(k) &= [z_{11}(k), \ldots, z_{bs}(k), \ldots, z_{N_{\text{steer}}N_{\text{bin}}}(k)]^{\text{T}} \\ &= \mathbf{h}(\mathbf{x}(k)) + \mathbf{v}(k)\end{aligned} \quad (3)$$

where $z_{bs}(k)$ is the expected energy observation corresponding to the sth time bin and the bth steering angle, $\mathbf{h}(\cdot)$ is the observation function that relates the state vector to the observations, and

$$\mathbf{v}(k) = [v_{11}(k), \ldots, v_{bs}(k), \ldots, v_{N_{\text{steer}}N_{\text{bin}}}(k)]^{\text{T}} \quad (4)$$

is the vector of uncorrelated Gaussian observation errors with zero mean and covariance matrix $\mathbf{R}(k) = \mathrm{diag}\left(\sigma^2_{11}(k), \ldots, \sigma^2_{bs}(k), \ldots, \sigma^2_{N_{\text{steer}}N_{\text{bin}}}(k)\right)$ with $\sigma^2_{bs}(k) = \mathrm{Var}\left(e_{bs}(k)\right)$. Note that the length $N_{\text{m}} = N_{\text{steer}}N_{\text{bin}}$ of $\mathbf{z}(k)$ is related either to the number of steering directions, depending on the TA pattern $G(\theta, f)$ characterized in the previous section, and to the number of time bins depending on the signal bandwidth W through T_{ED} [6].

The generic element of $\mathbf{z}(k)$ can be written as

$$z_{bs}(k) = h_{bs}(\mathbf{x}(k)) + \upsilon_{bs}(k) = \mathbb{E}\left[e_{bs}(k)\right] + \upsilon_{bs}(k) \qquad (5)$$

with $b = 1, 2, \ldots, N_{\text{steer}}$, $s = 1, 2, \ldots, N_{\text{bin}}$.
$\upsilon_{bs}(k)$ is the measurement noise, as defined in (4), with variance $\sigma^2_{bs}(k) = N_0(N_{\text{p}}WT_{\text{ED}}N_0 + 2T_{\text{f}}P_{bs}(k))$ and $N_0 = N_{\text{array}}\,\kappa \cdot T_0 \cdot N_{\text{F}}$, with κ being the Boltzmann constant, T_0 the receiver temperature, and N_{F} the receiver noise figure.

The term $\mathbb{E}\left[e_{bs}(k)\right]$ depends on $\mathbf{x}(k)$ as

$$\begin{aligned} P_{bs}(k) &= \frac{\mathbb{E}\left[e_{bs}(k)\right]}{T_{\text{f}}} = P_w \\ &+ \sum_{i \in \mathcal{R}(s)} \int_W \frac{P_t(f)\, c^2\, m_i^2(k)\, G^2(\theta_i - \theta_v - \theta_b, f) N_{\text{p}}}{f^2\, (4\pi)^3 d_i^4}\, df \end{aligned} \qquad (6)$$

where $P_t(f)$ is the transmitted power spectral density, $P_w = \frac{\sigma^2 T_{\text{ED}} N_{\text{p}}}{T_{\text{f}}}$ is the noise power with $\sigma^2 = N_0\, W$, d_i and θ_i are, respectively, the distance and angle between the TA and the ith cell. $\mathcal{R}(s)$ returns the set of cells indexes contributing to the sth time bin (i.e. all the cells located at a distance close to $s \cdot d_{\text{bin}}$ with $d_{\text{bin}} = c \cdot T_{\text{ED}}/2$).

IV. CASE STUDY

The case study here described refers to a typical indoor office environment of $20 \times 20\,\text{m}^2$, whose layout is juxtaposed to the estimated RCS maps in the results. As previously mentioned, we adopt a grid approach where the environment is discretized in cells having area $0.2 \times 0.2\,\text{m}^2$ each. We consider the radar equipped with a TA, exploring the surrounding area and collecting energy measurements by performing a scanning process over an angular range of $(-60°, 60°)$ as described in previous sections. The TA-radar moves along a determined and known path with a speed of 1 m/s and taking measurements every second. The path is indicated in Figs. 5 and 6; the black squares refer to the true TA-radar position while the green circles to the positions perceived by sensors. The orientation of the radar is always in the sense of the movement. The map estimation is performed by adopting the extended Kalman-Filter (EKF) method, as described in [5], to efficiently evaluate the posterior distribution $p(\mathbf{x}(k)|\mathbf{z}(1:k))$ of $\mathbf{x}(k)$ given the set of measurements $\mathbf{z}(1:k) = \{\mathbf{z}(1), \mathbf{z}(2), \ldots, \mathbf{z}(k)\}$ collected by the TA-radar until time instant k, from which a maximum a posteriori estimate of the state $\mathbf{x}(k)$ is derived.

We compare the TA mapping capabilities in terms of array size and focal distance degradation taking into account the quantization effect introduced by the discrete values of phase shifts. A 2-bit phase compensation is here adopted as a good compromise between maximum gain and TA unit-cells complexity.

A time frame of $T_{\text{f}} = 100\,\text{ns}$, $N_{\text{F}} = 4\,\text{dB}$, $T_0 = 290\,\text{K}$ and a signal bandwidth of $W = 1\,\text{GHz}$ ($T_{\text{ED}} = 1\,\text{ns}$) are considered. The time to complete an entire scan is fixed to $T_{\text{scan}} = 80\,\mu\text{s}$ while the number of steering directions and of pulses per interrogation signal varies with the number of antenna elements, i.e. $N_{\text{p}} = 81$, $N_{\text{p}} = 62$, $N_{\text{p}} = 21$ with $N_{\text{array}} = 10 \times 10$, $N_{\text{array}} = 15 \times 15$, $N_{\text{array}} = 20 \times 20$, respectively. Results are obtained considering an effective radiated isotropic power (EIRP) of 30 dBm in accordance to Federal Communications Commission (FCC) mask at 60 GHz [17]. Moreover, we consider a Lambertian scattering model and a wall made of aerate concrete by approximating the albedo with the power reflection coefficient, evaluated by setting the concrete relative permittivity to $\epsilon_r = 2.26$, its loss tangent to 0.0491 and its attenuation due to its thickness to 40 dB [18].

A. Numerical Results

Fig. 5 shows the RCS map estimation results considering a personal radar equipped with TAs of different size at $(F/D)_{\text{opt}}$ and without position and orientation errors. As can be seen, the mapping estimation accuracy increases with a higher number of antennas. In particular, an improved angular resolution is experienced with $N_{\text{array}} = 20 \times 20$ while the performance drastically decreases when $N_{\text{array}} = 10 \times 10$. In fact, the number of cells that are badly estimated is higher. Thus, a good trade-off between map's definition and TA complexity is represented by $N_{\text{array}} = 15 \times 15$, which guarantees good mapping performance while the personal radar complexity is kept affordable.
As previously discussed, another important parameter for array integrability in smart devices is the F/D ratio. Fig. 6-top shows the results obtained with $N_{\text{array}} = 15 \times 15$ and reduced F/D ratios, i.e. $F = 10\,\text{mm}$ and $F = 5\,\text{mm}$ instead of $F_{\text{opt}} = 19\,\text{mm}$. The reduced focal distance translates both in a gain degradation and in a larger main beam with a consequently reduction of the received signal-to-noise ratio (SNR) and of angular definition. Results for $F = 10\,\text{mm}$ show a slighter degradation of the mapping capability with respect to those obtained for F_{opt}. The effect of mobile radar positioning errors are investigated in Fig. 6-bottom where we have introduced orientation and position estimation errors with standard deviation of 5° and 0.1 m, both along the x- and the y- axis, respectively. It is evident from the figure how estimated maps become much more degraded even if the performance is still acceptable. Thus, if a key design parameter of the personal radar is represented by its compactness, which is the case when TAs have to be embedded into portable devices, $F = 10\,\text{mm}$ represents a valid and performing alternative to the solution with $F = F_{\text{opt}}$ which is less manageable.

V. CONCLUSIONS

The adoption of the mmW TA technology has been here proposed as an important solution to be embedded in personal

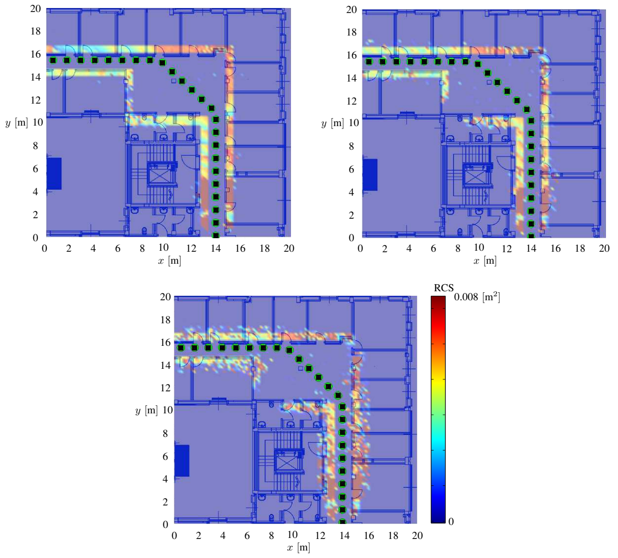

Fig. 5. Mapping results using 20×20 (top-left), 15×15 (top-right) and 10×10 transmitarray (bottom) with 2 bits phase compensation, optimal F/D ratio and with a perfect knowledge of TA-radar position and orientation.

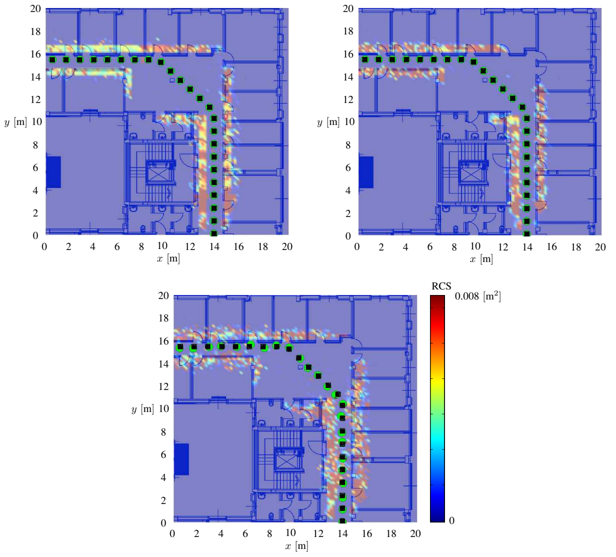

Fig. 6. Mapping results using 15×15 TA with a perfect knowledge of TA-radar position and orientation and with a reduced focal distance F = 10mm (top-left) and F = 5mm (top-right), and with TA-radar position and orientation errors and F = 10mm (bottom).

radars for environmental mapping. The performance of TAs has been investigated using an *ad-hoc* simulator experimentally validated at different bands. Different design parameters, such as the number of antenna elements, the focal distance, and the number of bits for phase compensation have been taken into account in the analysis. From this study, a 2-bit TA has been adopted for the mapping application because, in our opinion, it represents a good balance between complexity and radiation efficiency in view of the implementation of an electronically reconfigurable TA. The map reconstruction accuracy has been evaluated for different sized TAs and for reduced F/D values using a grid-based Bayesian state-space approach. Results have demonstrated that a 15×15 TA with a reduced focal distance of $F = 10$ mm permits to attain a good level of map reconstruction with the benefits of an easier integration and of a lower antenna array profile and cost. Future studies are oriented to characterize mmW TA mapping capabilities through measurements campaign in real office environments.

ACKNOWLEDGMENT

This work has been supported by the Italian Ministerial PRIN project GRETA (Grant 2010WHY5PR) and H2020 project XCycle.

REFERENCES

[1] C. Floerkemeier *et al.*, Eds., *The Internet of Things, First Int. Conf.* Springer, 2008.

[2] Y.-C. Lee *et al.*, "Artificial landmark map building method based on grid SLAM in large scale indoor environment," in *Proc. IEEE Int. Conf. on Syst. Man and Cybern. (SMC)*, Oct 2010, pp. 4251–4256.

[3] T. Rappaport *et al.*, in *Millimeter Wave Wireless Communications*. Prentice Hall, 2014.

[4] A. Guerra, F. Guidi, and D. Dardari, "Position and orientation error bound for wideband massive antenna arrays," in *Proc. IEEE Int. Conf. on Commun. (ICC), ANLN Workshop*, 2015.

[5] ——, "Millimeter-wave personal radars for 3D environment mapping," in *Proc. IEEE Asilomar Conf. on Signals, Systems, and Computers*, Pacific Grove, USA, Nov. 2014.

[6] F. Guidi, A. Guerra, and D. Dardari, "Millimeter-wave massive arrays for indoor SLAM," in *Proc. IEEE Int. Conf. on Commun. (ICC)*, June 2014, pp. 114–120.

[7] J. Huang and J. A. Encinar, *Reflectarray Antennas*. Hoboken, NJ USA: Wiley-IEEE Press, 2007.

[8] H. Kaouach *et al.*, "Wideband low-loss linear and circular polarization transmit-arrays in V-band," *IEEE Trans. Antennas Propag.*, vol. 59, no. 7, pp. 2513–2523, July 2011.

[9] A. Clemente *et al.*, "Multiple feed transmit-array antennas with reduced focal distance," in *Proc. 42nd European Microwave Conf. (EuMC)*, Oct 2012, pp. 826–829.

[10] L. Di Palma *et al.*, "Circularly polarized transmit-array with sequentially rotated elements in Ka band," in *Proc. 8th European Conf. on Antennas and Propag. (EuCAP)*, April 2014, pp. 1418–1422.

[11] J. Lau and S. Hum, "Reconfigurable transmitarray design approaches for beamforming applications," *IEEE Trans. Antennas Propag.*, vol. 60, no. 12, pp. 5679–5689, Dec 2012.

[12] P. Padilla *et al.*, "Electronically reconfigurable transmitarray at Ku band for microwave applications," *IEEE Trans. Antennas Propag.*, vol. 58, no. 8, pp. 2571–2579, Aug 2010.

[13] A. Clemente *et al.*, "Wideband 400-element electronically reconfigurable transmitarray in X band," *IEEE Trans. Antennas Propag.*, vol. 61, no. 10, pp. 5017–5027, Oct 2013.

[14] L. Di Palma *et al.*, "1-bit unit-cell for transmitarray applications in Ka-band," *Proc. 9th European Conf. on Antennas and Propag. (EuCAP)*, 2015.

[15] C.-C. Cheng, A. Abbaspour-Tamijani, and B. Lakshminarayanan, "Reconfigurable lens-array with monolithically integrated MEMS switches," in *Proc. 38th European Microwave Conf. (EuMC)*, Oct 2008, pp. 112–115.

[16] A. Clemente *et al.*, "Focal distance reduction of transmit-array antennas using multiple feeds," *IEEE Antennas Wireless Propag. Lett.*, vol. 11, pp. 1311–1314, 2012.

[17] "Revision of Part 15 of the Commissions Rules Regarding Operation in the 57-64 GHz Band," *Federal Communications Commission (FCC)*, Aug. 2013.

[18] L. Correia and P. Frances, "Estimation of materials characteristics from power measurements at 60 GHz," in *Proc. IEEE 5th Int. Symp. on Personal, Indoor and Mobile Radio Commun. (PIRMC)*, 1994, pp. 510–513 vol.2.